Biomedical Signal Processing and Control 79 (2023) 104172

Contents lists available at ScienceDirect

Biomedical Signal Processing and Control

journal homepage: www.elsevier.com/locate/bspc

CRCCN-Net: Automated framework for classification of colorectal tissue using histopathological images

Anurodh Kumar, Amit Vishwakarma *, Varun Bajaj

PDPM Indian Institute of Information Technology, Design and Manufacturing, Jabalpur, 482005, India

ARTICLE INFO

Keywords:
Colorectal cancer
Histopathological images
Pre-trained model
Convolutional neural network
Merged dataset

ABSTRACT

Colorectal cancer has a high mortality rate that continuously affects human life globally. Early detection of it extends human life and helps in preventing disease. Histopathological inspection is a frequently used approach to diagnose and detect colorectal cancer. Visual inspection of histopathological diagnosis requires more inspection time and the decision depends on the subjective perception of clinicians. This work proposed lightweight, less complex convolutional neural network-based architecture for automated classification of multi-class colorectal tissue histopathological images using two publicly available datasets, colorectal histology, and NCT-CRC-HE-100K, respectively. Histopathological images are provided as input to pre-trained models Xception, InceptionResNetV2, DenseNet121, VGG16, and the proposed network colorectal cancer classification convolutional neural network. This is the first study that compares the computational time of different deep learning architectures for the classification of colorectal tissue. The developed network requires less computational time for training compared to other pre-trained models. Accuracy, sensitivity, precision, false-positive rate, false-negative rate, specificity, F-1 score, and area under the curve have been used to evaluate the performance of the proposed architecture. The proposed network attained an accuracy of 93.50%, and 96.26% on the colorectal histology dataset, and NCT-CRC-HE-100K dataset, respectively. On the merged dataset, an accuracy of 99.21% is achieved by the newly developed network. The comparative analysis shows that the proposed framework outperformed existing state-of-the-art approaches. Clinicians may install the presented CRCCN-Net to confirm the diagnosis in the hospitals.

1. Introduction

According to global cancer statistics, colorectal cancer (CRC) is the third most common cause of death [1]. In 2022, American cancer society statistics estimated about 1.5 million will new CRC cases, and about 53000 deaths occur due to it, alone in the United States [2]. It occurs in the large intestine or rectum and is developed by unlimited cell division due to gene evolution. Polyps are mainly responsible for CRC. A polyp is a noncancerous swelling that grows slowly in the internal edging of the colon or rectum. Adenomatous and hyperplastic are the most common type of polyp. The adenomatous polyp has a more chance of getting cancer. Polyps that bring cancerous cells are known as malignant polyps.

The main causes of CRC include elderly age, polyposis, eating a lot of processed food, obesity, drinking too much alcohol and smoking, having a family history of colon cancer, and so on. Detection of CRC is a challenging task for clinicians and researchers. Many studies have been presented by scientists and researchers to aid in the early diagnosis of CRC. Fecal occult blood and fecal immunochemical are stool-based assessment tests followed by colonoscopy is the quality operation used to diagnose CRC and analyze the constructive impact. These physical inspections are usually unsafe since they do not account for the existential discrepancy, which reduces the overall effectiveness of cancer grading [3].

Medical imaging [4] is a crucial concept that takes part in the early diagnosis of CRC. Even with the increase in medical imaging data, it is challenging and time-consuming to analyze the data in relevance to the disease's rate of progression. Moreover, if misinterpretation of data is taken into consideration in the diagnosis of diseases, the performance of accuracy decreases and the period of early detection gets prolonged [5]. Therefore, the patients may be benefited from real-time, precise, and objective inspection results.

Histopathological inspection is a method used for the diagnosis of cancer. A microscope is used for histopathological inspection to determine the exact location and spread of the polyp. The histopathological diagnosis necessitates the aid of a clinical specialist, requires more inspection time, and the decision depends on the subjective perception

* Corresponding author.
E-mail addresses: anu.kumar823@gmail.com (A. Kumar), amitv@iiitdmj.ac.in (A. Vishwakarma), varunb@iiitdmj.ac.in (V. Bajaj).

https://doi.org/10.1016/j.bspc.2022.104172
Received 1 March 2022; Received in revised form 12 August 2022; Accepted 4 September 2022
Available online 28 September 2022

of clinicians. Automated detection of CRC using artificial intelligence may enhance the diagnosis performance and assist the clinicians in take their decision.

Various machine learning (ML)-based algorithms for the detection and classification of medical images have been explored in the literature. Entropy-based features have been widely extracted to detect different diseases and classification of biomedical signals. In [6], the authors analyzed the effect of music on the functioning of the human brain. They concluded permutation entropy is the suitable metric to identify the effects of sound on different temporal regions. In [7], the authors utilized a bidimensional empirical mode decomposition algorithm to decompose the mammographic images into different intrinsic mode functions. They extracted gray level co-occurrence matrix-based features from the intrinsic mode functions and classified them using the least square support vector machine (SVM) classifier.

Cross-validated classification algorithm has been employed to classify the emotion regulation strategies in resting-state using the spectral coherence technique [8]. Amin et al. [9] evacuated local binary pattern and Gabor wavelet transform-based features to detect the brain tumor. Tabesh et al. [10] extracted texture, morphometric cues, and color-based features using prostate tissue histopathological images (HIs), for the classification and grading of cancer. These reported ML-based methods for cancer detection to have two main limitations. First, extraction and selection of suitable features are time-consuming, as it is done on a trial-and-error basis. Second, various classifiers with many parameters have been used in earlier studies. Selecting an effective classifier is also a challenging task.

Nowadays, deep learning (DL)-based system is used to automatically extract the high-grade features from the input. It is a powerful tool to detect various health complications. A convolutional neural network (CNN) is a widely used DL architecture [11]. Various CNNs-based models have been explored for the detection and classification of biomedical signals and images. For example, the author in [12] explored the applications of the DL model to classify various emotional stages using electroencephalogram signals. In [13–16] authors also utilized the different DL architectures for the screening of various cardiac abnormalities. Cinar et al. [17] have proposed a hybrid of DenseNet121 and U-Net architecture for the segmentation of brain tumors from magnetic resonance images. Bratchenko et al. [18] have suggested a CNN model for skin cancer classification based on Raman spectra analysis. A fuzzy logic-based CNN model has been proposed by Nguyen et al. [19] for the detection of cancer.

In this paper, a colorectal cancer classification convolutional neural network (CRCCN-Net) has been proposed for the classification of multi-class colorectal tissue HIs. Four pre-trained models Xception, InceptionResNetV2, DenseNet121, VGG16, and CRCCN-Net have been trained separately on colorectal histology and NCT-CRC-HE-100K datasets, respectively. Further, these two datasets were merged and again trained with pre-trained models and CRCCN-Net to classify multi-class colorectal tissue HIs. The purpose of the merged dataset is to check the effectiveness of the proposed network on diverse datasets related to colorectal tissue HIs. Various performance parameters have been evaluated to obtain a deeper understanding of the proposed network. Finally, CRCCN-Net superiority has been evaluated by comparing it to the existing state-of-art methods on the same datasets. To summarize, the main contributions of the proposed work are as follows:

- This article proposed a lightweight, less complex CRCCN-Net to classify colorectal tissue HIs into multiple classes.
- To the best of the author's knowledge, this is the first study that compares the computational time of different DL architectures. Developed CRCCN-Net requires less computational time compared to other models.
- In this study, two different and one merged HIs datasets are utilized to compute the effectiveness, robustness, and stability of the developed CRCCN-Net. The proposed model attains a higher classification accuracy, sensitivity, precision, specificity, and F-1 score compared to the other networks.
- The robustness of the developed CRCCN-Net has also been tested on the lung cancer dataset to classify lung tissues into multiple classes.

The remaining part of the paper is summarized as follows: Section 2 depicts details of related work, Section 3 contains the materials and methods, Section 4 depicts the proposed method experiments and results, and Section 5 includes the discussion. In Section 6, the conclusion is presented.

2. Related work

This section discusses the previous ML and DL-based architecture to detect and classify colorectal tissue HIs. Rathore et al. [20] have extracted a combination of texture, color, morphological, and geometrical features using a hybrid feature space technique to classify malignant and normal classes of colon tissue. Hybrid feature space has been formed to the selection of a classifier with different types of discriminative features on the image texture and geometric structure. The performance has been evaluated on 174 images using various kernels of the SVM classifier.

A notable study has been proposed by Olgun et al. [21] to classify colon tissues HIs on texture-based features. They decomposed tissue images into hematoxylin and eosin components to achieve better classification accuracy. Tumor budding is a tiny tumor cell in CRC. For the classification and grading of cancer, Altunbay et al. [22] have proposed a color graph technique using histopathological colon patches. They extracted a new set of features from the color graph, and these features assisted in the classification of tissues using SVM. A biomarker is used to detect tumor buds for grading CRC. Physical assessment of tumor buds requires more time and may vary depending on the clinicians. Weis et al. [23] have suggested automatic detection of tumor buds using an SVM classifier.

Sirinukunwattana et al. [24] have proposed spatially constrained CNN to detect and classify colon cancer nuclei. They suggested a neighbor ensemble predictor in conjunction with CNN to predict the class label of detected nuclei with higher accuracy. The proposed methods for detecting and classifying nuclei did not necessitate nuclei segmentation [24]. The performance has been evaluated on 20,000 annotated nuclei images among four different classes. The results obtained through their proposed method could benefit pathologists in the analysis of colorectal tissue HIs. The limitation of their work was related to the empirical selection of hyperparameters in the proposed CNN.

Sari et al. [25] have proposed a DL-based algorithm to classify colon tissue histological images. They presented an unsupervised feature extractor for the constructive representation and classification of colon tissues. Their proposed method has been tested on two different datasets of colon tissue HIs. The local deep features extracted by the model produced better classification results, except for classes having comparably large non-epithelial regions.

Bilinear CNN has been developed by Wang et al. [26] for the classification of eight class colorectal tissue HIs. The authors first decomposed HIs into hematoxylin and eosin stain components. Then, performed bilinear CNN on decomposed images to learn more effective features. The limitation of their work was that they considered 1000 images (for training, validation, and testing) out of 5000 images of a dataset. Moreover, the information about bilinear CNN architecture such as the number of convolutional layers, and kernel size is not mentioned.

Kather et al. [27] have proposed a DL-based architecture that assesses tumor microenvironment from HIs. The authors have evaluated the performance of five pre-trained models, namely, AlexNet, GoogleNet, SqueezeNet, ResNet50, and VGG19, which have trained on the ImageNet dataset [27]. They have trained these pre-trained models on 100 K image patches taken from 86 CRC patients, to classify nine different classes of colorectal tissues. The performance of their method

has been tested on a different dataset of 7180 colorectal image patches from 25 CRC patients. The classification results of VGG19 were better as compared to other pre-trained models. In this work, misclassification was very common between a few classes of colorectal tissue.

Liang et al. [28] have proposed multi-scale feature fusion CNN (MFF-CNN) based on shearlet transform, for the identification of colon cancer. The advantage of their suggested method was the use of the shearlet coefficient obtained by applying the shearlet transform on HIs. The shearlet coefficients consist of additional features related to edges, contours, etc. These features were also given along with the input HIs images to the network. Although shearlet transform is well localized and highly directive. However, shearlet elements with large shearing parameters suffer from shift variance and directional bias. This study has considered only two classes out of nine classes of the dataset.

Ghosh et al. [29] have developed an ensemble deep neural network (DNN) for the classification of multi-class colorectal tissue HIs. The authors have suggested three pre-trained networks, namely, DenseNet121, Xception, and Inception-ResNetV2 along with a configurable CNN. These CNNs weights were transferred to ensemble DNN and then trained on two different datasets, separately. Various performance metrics have been evaluated to check the efficacy of CNNs. Their proposed method achieved better performance than previously reported results on the same datasets [29]. The limitation of their work is ensembling may be expensive in terms of space and time. The paper also did not provide clear information about the configurable CNN, such as the number of convolutional layers and filters used at each layer, and kernel size.

Hamida et al. [30] have proposed a DL-based approach to classify and highlight CRC regions in sparsely annotated histological data. They have compared various CNNs namely, VGG, AlexNet, ResNet, DenseNet, and Inception in their study. ResNet achieved better performance than other pre-trained networks on different datasets related to colorectal tissue. They also suggested a pixel-wise segmentation approach for CRC whole slide images using UNet and SegNet. The limitation of their study is that the models underperformed if the whole slide image encloses small regions of nearby classes at each patch. Also, these CNNs are usually required more time for training.

Interactive learning and attention mechanism-based approach have been suggested by Chen et al. [31] for the classification of colorectal tissue HIs. Their proposed framework comprises two stages, namely, automatic learning and interactive learning. In the automatic learning stage, a multi-channel attention mechanism model with three separate attention mechanism channels and CNNs was utilized to extract multiple channel features for the classification of colorectal tissues. In the interactive learning stage, their framework consistently adds misclassified HIs to the training set in an interactive way, which boosts the classification results of their proposed model. The limitation of their suggested approach is that it increases the number of weight parameters in the model which may increase training and testing time.

For diagnosis of CRC using HIs, Sabol et al. [32] have proposed a cumulative fuzzy class membership criterion classifier for enhancing the decision-making ability of the model. Their suggested model does not clarify the reason between the input and decisions but provides a better explanation of the rationality in taking decisions. Various pre-trained CNNs have been used to compare the proposed classifier in terms of accuracy, for the classification of eight class colorectal tissue HIs. The limitation of their work is their suggested model had not been tested on imbalanced and heterogeneous datasets.

Kwak et al. [33] have proposed a deep CNN-based model to predict lymph node metastasis for diagnosis of colon cancer. Their developed model used the peritumoral stroma score for the prediction of lymph node metastasis. The limitation of their approach is the dataset used may be biased in terms of typically containing images, in which the morphological structure is conclusive.

For the classification of CRC histological images transfer learning approach has been applied using various pre-trained CNNs in [34]. The features have been extracted from various pre-trained CNNs, and extracted features are given as input to various (Random forest, Naive Bayes, k-Nearest Neighbors, SVM) classifiers. Their method used 5000 images of eight different types of colorectal tissues. DenseNet-169 with SVM classifier using radial basis function achieved better performance as compared to some pre-trained CNNs. The limitation of their work is the proposed method has been used on a single and balanced dataset.

Wang et al. [35] have proposed a DL-based technique for the diagnosis of CRC. They proposed a patch aggregation strategy using weakly labeled whole slide image patches. The suggested approach was trained and validated using an enormously large number of image patches on diverse datasets. Inception-v3 architecture has been utilized to classify normal and cancerous image patches. Inception-v3 is a complex CNN architecture as it uses more layers and trainable parameters.

A DL-based detailed review article has been published by Davri et al. [36] for CRC diagnosis using HIs. The authors have focused on the inspection from technical and medical viewpoints. Their contribution to the systematic review presented an extensive analysis of DL-based models for the diagnosis of CRC. Their study demands the DL-based model in the diagnosis of CRC and various types of cancer such as lung, breast, prostate, etc.

Most of the existing DL models have large sizes, more learnable parameters, require more training time, are trained on a single dataset, and give less classification performance. Moreover, the main issue in most of the existing DL-based approaches is to find the optimal capacity of the model. A model with higher capacity leads to overfitting and a model with lower capacity leads to underfitting. The proposed model is designed such that the capacity of the model is near optimal because the difference between training and test accuracy is approximately 1.5%, while both accuracies are on the higher side. The existing models were more specifically built for a certain use case, and may not always be best suitable for medical image classification such as HIs and other image modalities. The main objective of this work is to design a comparatively lightweight, less complex deep learning model for the efficient classification of colorectal tissue HIs for the screening of CRC. The number of layers and number of filters in each layer in the presented CRCCN-Net is chosen experimentally. As a result, developed CRCCN-Net requires less time for training and attains a stable and faster response.

3. Materials and methods

The most important aspects in histological imaging for diagnosing CRC are cell nuclei appearance, nucleus to cytoplasm ratio, cyst geometry, and tissue appearance. In this work, four pre-trained models, namely, Xception, InceptionResNetV2, DenseNet121, VGG16, and proposed CRCCN-Net are used for the automatic classification of colorectal tissue HIs.

3.1. Datasets

The two publicly available datasets are epitomized as follows:

1. Colorectal histology: The dataset is available on https://zenodo.org/record/53169#.Yp86-nZBzIX. The pathology archive at the University Medical Center Mannheim (UMM), Germany provided 10 confidential hematoxylin and eosin stained CRC tissue slides. This group comprises both low-grade and high-grade tumors. The colorectal histology dataset [37] comprises 5000 image tiles of size 150 × 150 pixels and correspondingly distributed into eight non-overlapping classes, namely DEBRIS (DEB), ADIPOSE (ADI), STROMA (STR), MUCOSA (MUC), EMPTY (EMP), LYMPHO (LYM), TUMOR (TUM), and COMPLEX (COM). All images are RGB channel format with 20 × magnification. Fig. 1 depicts the image patches for each class. In the later part of this paper, the colorectal histology dataset is renamed Dataset_1.

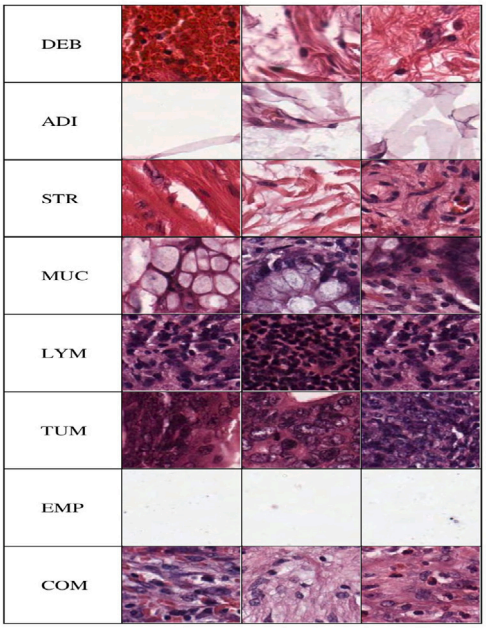

Fig. 1. Depiction of eight class colorectal histology dataset.

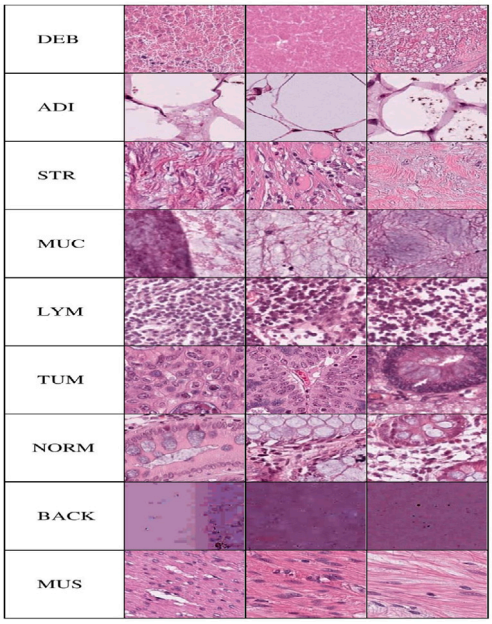

Fig. 2. Depiction of nine class NCT-CRC-HE-100K dataset.

2. NCT-CRC-HE-100K: The dataset is available on https://zenodo.org/record/1214456#.Yp9BY3ZBzIU. This dataset [38] comprises 100,000 hematoxylin and eosin stained images of CRC and normal tissue, each having a size of 224 × 224 pixels. Normal tissue classes were supplemented with non-tumorous regions from gastrectomy specimens to increase variability. This dataset comprises nine classes. The defined classes are lymphocytes (LYM), debris (DEB), background (BACK), mucus (MUC), cancer-associated stroma (STR), smooth muscle (MUS), normal colon mucosa (NORM), adipose (ADI), and colorectal adenocarcinoma epithelium (TUM). Each class signifying tumor containing regions. CRC-VAL-HE-7K is a collection of 7180 image patches from 50 CRC patients, with no overlap with patients in NCT-CRC-HE-100K. It can be used to test models that have been trained on the larger dataset. Fig. 2 depicts the image patches for each class. In the later part of this paper, the NCT-CRC-HE-100K dataset is renamed Dataset_2.

This work emphasized using the datasets mentioned above since they both contain comparable data files, and merging them provides a more number of images, making it more ideal for DL applications [29]. This work used two datasets, namely, Dataset_1, and Dataset_2. Dataset_1 comprises eight classes, namely DEB, ADI, STR, MUC, LYM, TUM, EMP, and COM. Dataset_2 comprises nine classes, namely DEB, ADI, STR, MUC, LYM, TUM, NORM, BACK, and MUS. As in both datasets, the initial six classes are common. Therefore, both datasets are merged. Before merging both datasets EMP class is discarded from the Dataset_1 as this class images have null information. After merging both datasets, the merged dataset is obtained. The images obtained from the merged dataset comprise ten classes, namely DEB, ADI, STR, MUC, LYM, TUM, COM, NORM, BACK, and MUS. After merging both datasets 1,11,555 images are obtained. In the later part of this paper, the merged dataset is renamed Dataset_3. The images obtained from Dataset_3 are divided into three categories: training (80%), test (12%), and validation (8%), and the same method is used for training with separate datasets. All HIs are resized to 128 × 128 before being provided as an input to CNNs.

3.2. Convolutional Neural Networks (CNNs)

CNN is widely used for image classification, object identification, computer vision, face recognition, emotion recognition, and so on [39–42]. CNN is formed by a convolutional layer (CL), a pooling layer (PL), a nonlinear transform layer, and a fully connected layer (FC). CLs and PLs extract features from the input images, while the FC layer is used for the classification task. An activation function is utilized along with convolution. The activation function enhances the networkôs nonlinearity. Rectified linear unit (ReLu) is the most frequently used activation function. PL is also called the subsampling layer. The purpose of the PL is to preserve important information while reducing the size and parameters. The output of the PL is provided to the FC layer.

Convolution is used in conjunction with an activation function. The activation function boosts the network's nonlinearity. Rectified linear unit (ReLu) is the most commonly utilized activation function. ReLu activation function overcomes the vanishing gradient problem, allowing models to learn faster and perform better. It provides good results in image classification tasks as present in some well-known classification models and is also used for fast convergence [15,43]. The PL also known as the subsampling layer, succeeds the CL. The main purpose of the PL is to use downsampled feature maps. It keeps important information while reducing the parameters and size. The output of the PL is fed to the FC layer.

A 2-D feature map is converted to a 1-D feature map using the FC layer. The softmax layer translates the score into probabilities, and the classification layer assigns a class to an object based on an algorithm. Overfitting may exist during training CNN-based models. Dropout is acquired to reduce overfitting problems, which irregularly drop features. Batch normalization, which examines the mean and variance for a mini-batch category, is also used to improve network performance. CNN with batch normalization learns faster and improves accuracy.

Many pre-trained deep CNNs have been used for various artificial intelligence challenges to developments in CNN, such as AlexNet, VGG16, SqueezeNet, ResNet, and GoogleNet. These networks transfer their prior knowledge grasped skills from one domain to another to extract features and classification. In this paper, four pre-trained CNN Xception, InceptionResNetV2, DenseNet121, and VGG16 have

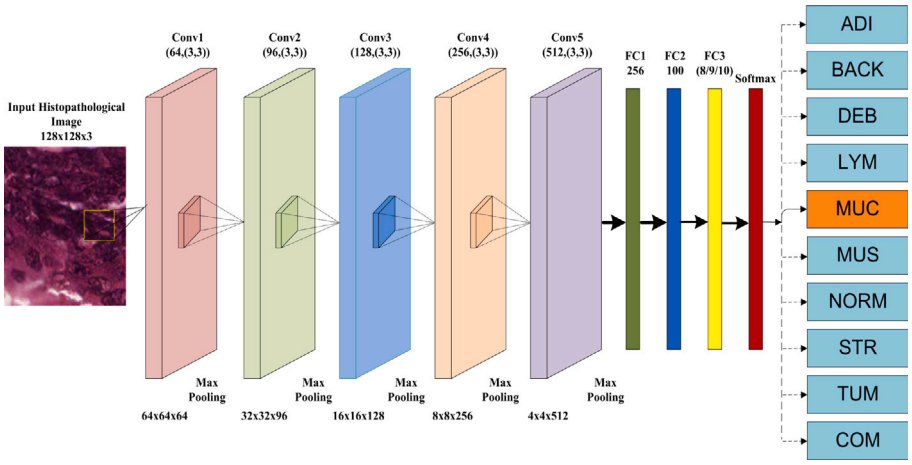

Fig. 3. Network architecture of CRCCN-Net.

been used for colorectal tissue HIs classification. Xception is a deep CNN framework of an extended version of Inception. The network contains an adjusted deepness distinguishable convolution which is an amalgamation of depth-wise and point-wise convolution.

Xception consists of an image size of 299 × 299 and 36 CLs arranged into 14 blocks. InceptionResNetV2 is combination of Inception and ResNet networks. Each inception block is followed by a filter expansion layer, which expands the dimensions of the filter bank, and the amalgamation of these two networks boosts the model's performance even further. The network has 164 layers and a 299 × 299 input size. DenseNet121 network uses feature maps to transport data from one layer to the next in a sequential manner. Batch normalization, ReLu layers and dense blocks, transition layers, and the final compression layer are all supported by a sequence of completely connected levels, starting with a fundamental composition layer. The network has an input image size of 224 × 224. VGG16 is a well-known and widely utilized pre-trained network used to evaluate the system's performance. It takes an image with a size of 224 × 224 pixels as an input. It has a filter size of 3 × 3 and consists of 16 CLs and three FC layers. The details of the above network are found in [39–42].

3.2.1. CRCCN-Net

Most of the used CNN models have bulky structures. Therefore, these models consist of more learnable parameters which require more training and testing time. Moreover, these higher capacity models may give less generalization classification performance. The selection of hyperparameters has a big impact on CNN's performance. The number of layers can be increased or decreased at the user's discretion [44]. Classification accuracy can be adjusted by changing the filter size, dropout, stride, and other parameters [43]. Fig. 3 depicts the network architecture of CRCCN-Net.

The strength of the proposed network is the number of filters used at each CL and the use of three FC layers. For any network, the more filters used at each CL, the more features can be extracted from raw images. In most of the pre-trained CNNs, the number of filters may range from 32 to 1024 at each CL. But, more filters at each CL, increase the number of learnable parameters which may take a long time to train a network. To keep these things in mind the proposed network is designed. In the proposed network, there are 64, 96, 128, 256, and 512 filters used at respective CLs, that use less trainable parameters and improve the classification accuracy. Also, if datasets have multiple classes or if the classes are similar to each other, the relationship between them during network training may be very close. Hence, for better classification accuracy of the proposed network three FC layers are used.

CRCCN-Net comprises five CLs, five PLs, three FC layers, and one softmax layer. In the proposed network 64, 96, 128, 256, and 512 filters are used at first CL, second CL, third CL, fourth CL, and fifth CL, respectively. For each CL 3 × 3 filter size is used. The CLs are padded to assure the output has a features map that is identical to the inputs. Max-pooling operation is used in PL to reduce the parameters, and size and preserve the important information. ReLu activation function is used at each CL to boost the network nonlinearity. After five CLs and PLs, a flattening layer combines the output into the feature vector.

The feature vector is transferred to three FC layers FC1, FC2, and FC3 respectively. FC1 and FC2 layers consist of 256 and 100 neurons, respectively. The number of neurons in FC3 is similar to the number of output classes. In FC3 the number of neurons is 8, 9, and 10 for the Dataset_1, Dataset_2, and Dataset_3, respectively. CRCCN-Net has the same number of output nodes as the number of classes. Each output node is associated with a class and provides a score for that class. The scores from the previous layer are passed via a softmax layer, which converts the scores into probability values. The softmax layer's probabilities are also utilized to calculate the loss during training and to find the predicted class during testing.

In Fig. 3, the input histopathological image belongs to the MUC class. MUC is highlighted in a different color as the proposed network correctly predicts the outcome of the histopathological image given as an input. In addition, CRCCN-Net requires lower learnable parameters than used pre-trained CNN architecture Xception, InceptionResNetV2, DenseNet121, and VGG16, respectively. The number of layers and number of filters in each layer in the presented CRCCN-Net is chosen experimentally. Based on various experiments proposed network attained the highest efficacy for the above combination. Although a layered architecture with more layers performed better than with fewer layers, increasing the layers and neurons beyond the proposed number did not improve the network's performance [45].

3.2.2. Mathematical model

The 2-D convolution operation is computed as Eq. (1)

$$(W \otimes H)(m,n) = \sum_{i,j} W(i,j)H(m+i,n+j) \tag{1}$$

The stride (s) is usually used to move the filters. At times, zero paddings (t) are also applied to maintain the image size. For an input image size $B{\times}H{\times}C$, where B represents width, H denotes height, and C represents channel numbers. With N_0 filters having size $h \times h$, the output size can be given as Eq. (2)

$$\begin{aligned} B_0 &= \frac{B-h+2t}{s}+1 \\ H_0 &= \frac{H-h+2t}{s}+1 \end{aligned} \tag{2}$$

ReLu is used as an activation function and is given as Eq. (3)

$$ReLu(x) = max(0,x) \tag{3}$$

The PL is used to reduce the feature maps and also aids in the prevention of overfitting. Max pooling operation is the most commonly used pooling operation. The output maps are normally lower than the input maps and given by Eq. (4)

$$y_j^k = f(\gamma_j^k low(\gamma_j^{k-1}) + \delta_j^k) \tag{4}$$

where γ_j^k denotes the multiplicative bias, δ_j^k represents the additive bias, and $low(\cdot)$ shows the pooling function. The output of the PL is fed to a flattening layer that combines the output into the feature vector. The feature vector is transferred to three FC layers FC1, FC2, and FC3, respectively for the classification of colorectal tissue. Algorithm 1 describes the process involved in the proposed CRCCN-Net.

Algorithm 1 : Framework for CRCCN-Net algorithm

Training Process

Input: Histopathological Images ($B\times H\times C$), Learn_rate, Batch_size, Num_layers, Filter_size (3×3)
I_pre= Preprocess ($B\times H\times C$)
model = create_model (Num_layers, Filter_size, Batch_size, Learn_rate)
CRCCN-Net = Train(I_pre,model)

Classification Process

Input: I_test ($B\times H\times C$)
Ipretest = preprocess I_test ($B\times H\times C$)
classifier output = CRCCN-Net(Ipretest)
Output = classifier output

3.2.3. Training period

During the training period, the categorical cross-entropy/log loss is evaluated. The weights of the network have reformed by finding the gradient of parameters with respect to the loss function. The log loss is utilized to evaluate the performance of a classifier whose output is a probability score ranging between 0 and 1. Let $B\times H\times C$ be an input histopathological image, to the proposed network with class label $g \in G$ where $G = \{g_1, g_2, g_3 \cdots \cdot g_n\}$ is the set of class labels. In this work, $G = \{1, 2, 3 \cdots \cdot 8\}$ for Dataset_1, $G = \{1, 2, 3 \cdots \cdot 9\}$ for Dataset_2, and $G = \{1, 2, 3 \cdots \cdot 10\}$ for Dataset_3. The network's output is a vector O which is given in Eq. (5)

$$O = f(B \times H \times C) \tag{5}$$

where $O = \left[O_1, O_2, O_3 \cdots \cdot O_{g_k}\right]$ shows the class score for the k classes and f represents the forward pass function. $B\times H\times C$ in Eq. (5) represents size of the input image size, where, B, H, and C depict the width, height, and the number of channels, respectively. If the target class is g_i the cross-entropy loss for $B\times H\times C$ is given as Eq. (6)

$$L = -log\left(\frac{e^{O_i}}{\sum_{k=g_1}^{g_n} e^{O_k}}\right) \tag{6}$$

where L represents the categorical cross-entropy loss.

3.2.4. Testing period

The predicted class label for an input image is the class label with the highest scores at test time. In Eq. (6) i denotes the number of classes. For Dataset_1, i varies from 1 to 8, for Dataset_2 i varies from 1 to 9, and for Dataset_3 the range of i is 1 to 10. The predicted class label g_j can be calculated as Eq. (7).

$$g_j = \underset{i}{argmax}\, p\left(O_i\right) \tag{7}$$

where $p\left(O_i\right)$ is the probability that $B\times H\times C$ belongs to class g_i, which can be calculated as Eq. (8)

$$p\left(O_i\right) = \frac{e^{O_i}}{\sum_{k=g_1}^{g_n} e^{O_k}} \tag{8}$$

4. Experiments and results

This section discusses an experimental analysis of Dataset_1, Dataset_2, and Dataset_3 to classify colorectal tissue HIs. Comparative analysis of four pre-trained models Xception, InceptionResNetV2, DenseNet121, VGG16, and proposed CRCCN-Net, are described with various performance metrics. Finally, the efficacy of the presented network is demonstrated with other existing methodologies for the classification of colorectal tissue HIs. Table 1 lists the layers that are required and the total trainable parameters for each layer.

Table 2 depicts the total trainable parameters used in various models. From Table 2, it can be seen that CRCCN-Net required comparatively lesser parameters as compared to other pre-trained models. Hence, the proposed network is lightweight. To check the performance of CRCCN-Net following performance metrics are evaluated: accuracy (Acc), sensitivity (Sen), precision (Pre), specificity (Spe), F-1 score, an area under the curve (AUC), false-positive rate (FPR), and false-negative rate (FNR). If there are unbalanced samples in each class or dataset, then multiclass classification accuracy alone can be misleading. Hence, various metrics have been used to check the efficacy of the proposed CRCCN-Net.

4.1. Implementation details

All networks have been trained using Adam optimizer with different hyperparameters. Adam optimizer combines the best aspects of RMSProp and AdaGrad algorithms while using less memory [46]. The required values were set to 0.9 for the first moment, 0.999 for the second moment, and 0.8 for the decay. A typical value of dropout ranges from 0.2 to 0.5 [47]. In the proposed method, a dropout of 0.2 is considered because this value prevents the model from getting overfit and underfit. All of the experiments have been performed on a computer with an Intel(R) Core(TM) i7-3770 CPU@3.40 GHz and 24 GB RAM, and the suggested approach has been implemented in Python 3.8 using Keras and Tensorflow. Table 3 represents the performance evaluation of CRCCN-Net using various learning rates and batch sizes on the different datasets. Throughout the experiment, a uniform filter of size 3×3 has used. From Table 3, it can be seen that the proposed network achieved the best classification accuracy on different datasets, for a batch size of 64, and a learning rate of 0.0001.

4.2. Experimental results on Dataset_1

The dataset and proposed network are described in Section 3. HIs are given as input to four pre-trained models and CRCCN-Net to test the performance of the developed approach. The proposed network automatically extracts multi-resolution features from HIs of colorectal tissue with lower trainable parameters than four pre-trained CNNs. The softmax layer has been used at the output of these networks. Dataset_1 has been trained on 5000 HIs which is relatively fewer samples to train a deep network. Hence, for better training, the CNNs have been trained to more epochs using early stopping. The early stopping criterion is used to stop training when a monitored metric (loss) has stopped improving. Fig. 4 shows the training and validation loss plot of CRCCN-Net, and Fig. 5 represents the training and validation accuracy plot of CRCCN-Net. These plots depict how the network is trained and how rapidly it converges over the epochs.

Confusion matrix obtained for Dataset_1 is shown in Fig. 6. Furthermore, Xception, InceptionResNetV2, DenseNet121, and VGG16, are used to compare the performance of CRCCN-Net. The results of the test dataset after training and validation for all networks are shown in Table 4. CRCCN-Net has a more significant influence on the test dataset than four pre-trained models. The receiver operating characteristic curve is shown in Fig. 7 of the proposed network.

Table 1
Tunable parameters used in CRCCN-Net.

S. NO.	Layer	Number of filters	Filter size	Total trainable parameters
1	Conv2D	64	3 × 3	1792
2	Max-pooling	–	2 × 2	0
3	Conv2D	96	3 × 3	55392
4	Max-pooling	–	2 × 2	0
5	Conv2D	128	3 × 3	110720
6	Max-pooling	–	2 × 2	0
7	Conv2D	256	3 × 3	295168
8	Max-pooling	–	2 × 2	0
9	Conv2D	512	3 × 3	1180160
10	Max-pooling	–	2 × 2	0
11	FC1	–	–	2097408
12	FC2	–	–	25700
13	FC3Softmax	–	–	(808/909/1010)

Table 2
Total trainable parameters used in various models.

Model	Total trainable parameters (Approx. in Millions, M)
Xception	22.8 M
InceptionResNetV2	54 M
DenseNet-121	20 M
VGG16	138 M
CRCCN-Net	**3.76 M**

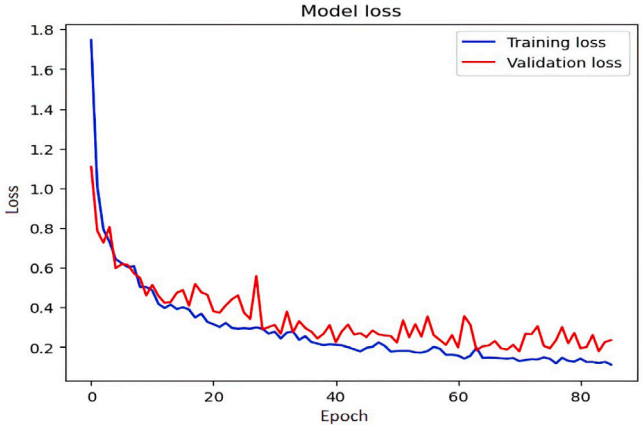

Fig. 4. CRCCN-Net training and validation loss on Dataset_1.

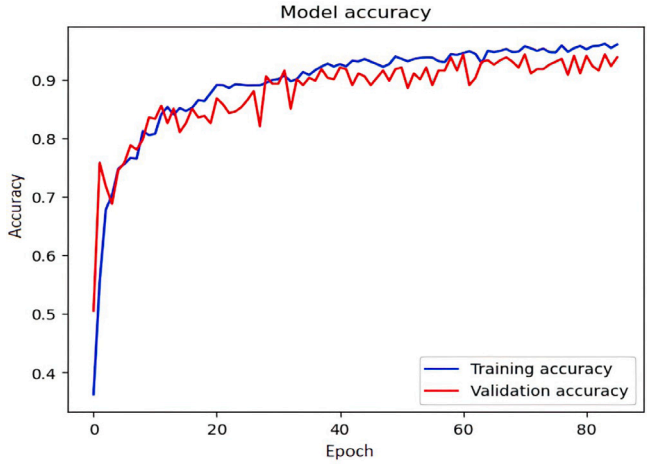

Fig. 5. CRCCN-Net training and validation accuracy on Dataset_1.

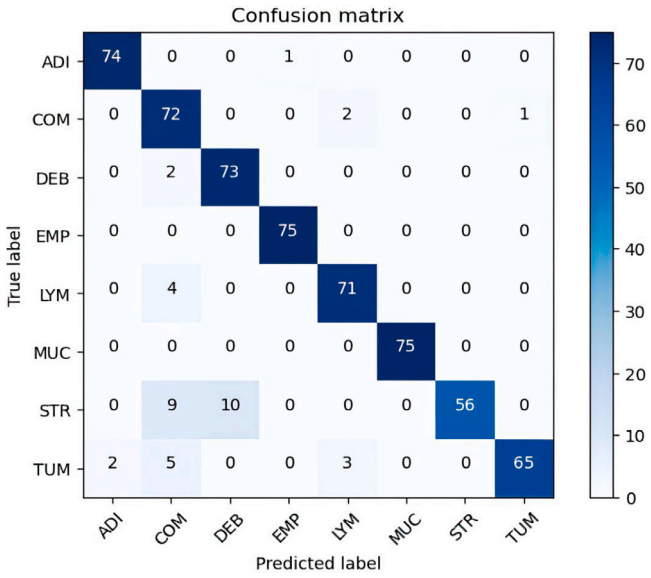

Fig. 6. Confusion matrices obtained from external test data using CRCCN-Net on Dataset_1.

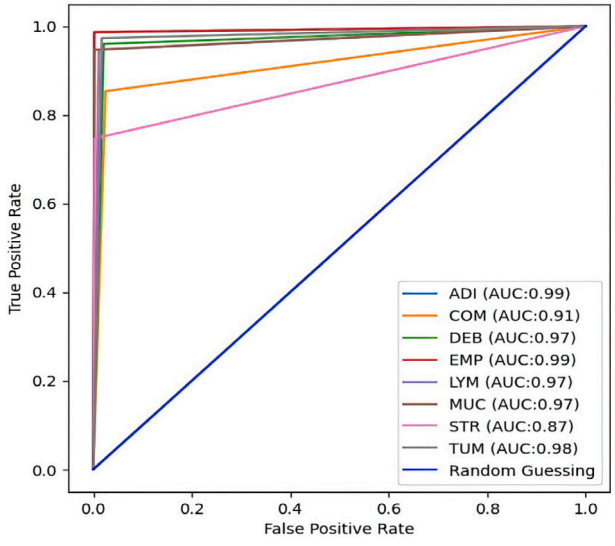

Fig. 7. Receiver operating characteristic of Dataset_1.

Table 3
Performance evaluation of CRCCN-Net using various hyperparameters on the different datasets using a uniform filter size 3 × 3.

Batch size	Learning rate	Number of filters	Dataset_1 Acc(%)	Dataset_2 Acc(%)	Dataset_3 Acc(%)
32			86.14	92.82	97.05
64	0.001	32, 64, 128	86.84	93.24	97.14
128			86.56	93.27	97.08
32			86.74	93.84	97.08
64	0.0001	32, 64, 128	87.62	93.92	97.10
128			87.56	93.67	96.82
32		32, 64,	89.34	94.56	97.05
64	0.001	128, 256	89.36	94.70	97.18
128			89.22	94.38	97.36
32		32, 64,	89.24	94.30	97.22
64	0.0001	128, 256	89.84	94.68	97.36
128			89.80	94.56	96.98
32		64, 96,	91.93	95.14	97.68
64	0.001	128, 256, 512	92.86	95.46	98.10
128			92.36	95.06	97.88
32		64, 96,	93.08	95.88	98.84
64	**0.0001**	128, 256, 512	**93.50**	**96.26**	**99.21**
128			93.22	96.10	98.68
32		32, 64, 96,	92.08	95.24	97.46
64	0.001	128, 256, 512	91.56	95.64	97.75
128			91.34	95.43	98.16
32		32, 64, 96,	92.46	96.08	98.37
64	0.0001	128, 256, 512	92.68	96.12	98.87
128			92.28	95.98	98.64

Table 4
Performance evaluation on Dataset_1 for individual model.

Parameters	Xception	Inception-ResNetV2	DenseNet 121	VGG16	**CRCCN-Net**
Acc (%)	88.20	89.20	87.20	90.40	93.50
Sen(%)	86.80	87.90	85.68	89.03	93.62
Pre (%)	87.40	91.40	84.78	89.88	94.12
Spe (%)	88.28	93.27	86.83	94.23	99.06
FPR (%)	10.76	7.20	10.87	8.68	0.92
FNR (%)	11.20	9.85	10.34	9.17	6.49
F-1 Score	0.8709	0.8961	0.8522	0.8945	0.9386
AUC	0.9135	0.9234	0.8972	0.9368	0.9573

4.3. Experimental results on Dataset_2

The dataset and proposed network are described in Section 3. On Dataset_2, four pre-trained networks have been compared with CRCCN-Net for the classification of colorectal tissue using HIs. After training and validation, CRCCN-Net substantially impacted the test dataset compared to all pre-trained CNNs. All networks have been trained to 30 epochs.

Figs. 8 and 9 show the training and validation loss and training and validation accuracy of CRCCN-Net, respectively. These plots represent how the model is trained and how rapidly it converges over the epoch. The confusion matrix obtained for the Dataset_2 is shown in Fig. 10. Fig. 11 shows the receiver operating characteristic curve of CRCCN-Net. Table 5 depicts the results of the test dataset after training and validation for all networks. Table 5 shows that CRCCN-Net has a significant influence on the test dataset than four well-trained CNNs.

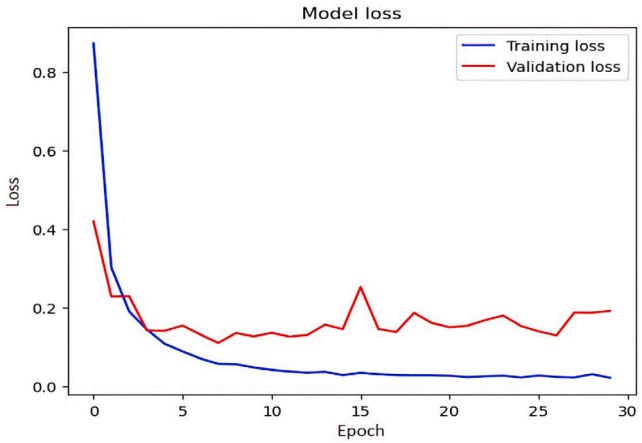

Fig. 8. CRCCN-Net training and validation loss on Dataset_2.

4.4. Experimental results on Dataset_3

The details about the dataset and proposed approach are described in Section 3. 30 epochs have been used to train four pre-trained networks and CRCCN-Net. Merging the datasets, networks are adjusted to new feature examples. The networks have a greater chance of identifying hidden patterns in more data samples. As a result, merging the datasets yields better results as compared to training them separately.

Batch normalization with momentum 0.8 has been added to normalize the output of the CL and minimize overfitting. Further, four pre-trained CNNs along with CRCCN-Net have been compared on Dataset_3. After training and validation, CRCCN-Net significantly affected the performance of pre-trained networks on test datasets to classify colorectal tissue. Fig. 12 shows the training and validation loss of CRCCN-Net, and

Table 5
Performance evaluation on Dataset_2 for individual model.

Parameters	Xception	Inception-ResNetV2	DenseNet 121	VGG16	**CRCCN-Net**
Acc (%)	94.18	91.26	92.34	95.74	96.26
Sen (%)	92.74	90.78	91.12	94.98	96.34
Pre (%)	94.80	92.89	90.74	94.26	96.44
Spe (%)	96.28	90.08	92.86	97.68	99.52
FPR (%)	8.18	11.64	8.68	6.22	4.60
FNR (%)	9.76	8.75	10.24	5.74	3.79
F-1 Score	0.9375	0.9182	0.9092	0.9461	0.9638
AUC	0.9448	0.8912	0.9238	0.9622	0.9781

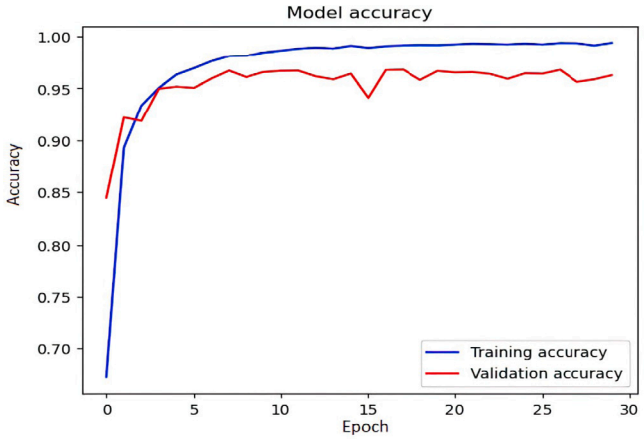

Fig. 9. CRCCN-Net training and validation accuracy on Dataset_2.

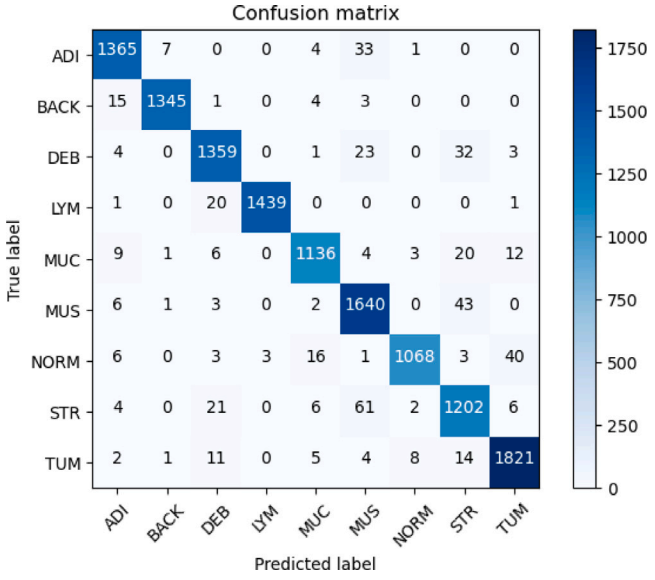

Fig. 10. Confusion matrices obtained from external test data using CRCCN-Net on Dataset_2.

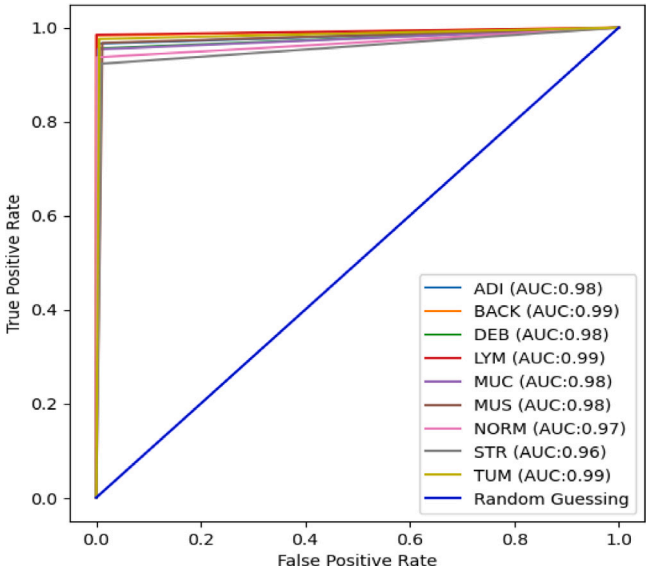

Fig. 11. Receiver operating characteristic of Dataset_2.

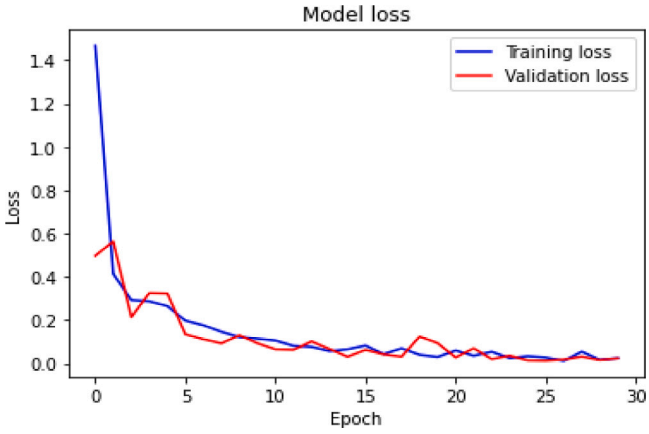

Fig. 12. CRCCN-Net training and validation loss on Dataset_3.

Fig. 13 represents the training and validation accuracy of CRCCN-Net. The confusion matrix obtained for Dataset_3 is shown in Fig. 14.

CRCCN-Net performance has compared to that of four pre-trained models, namely, Xception, InceptionResNetV2, DenseNet121, and VGG16. From Table 6, it can be observed that CRCCN-Net has a higher effect on the test dataset in comparison with four pre-trained models. The receiver operating characteristic curve is shown in Fig. 15 of CRCCN-Net.

Table 7 depicts the training time of different models in minutes per 30 epochs on two different and one merged dataset. CRCCN-Net requires approximately 58, 1622, and 1810 min to train, on Dataset_1, Dataset_2, and Dataset_3, respectively. From Table 7, it can be observed that CRCCN-Net outperformed as compared to four pre-trained models in terms of computational time complexity.

5. Discussion

Precise diagnosis of CRC is the need of the hour, most of the existing CNN models have large sizes, use more learnable parameters, require more training time, and give less classification performance. Developed CRCCN-Net can aid pathologists with an upgraded clinical

Table 6
Performance evaluation on Dataset_3 for individual model.

Parameters	Xception	Inception-ResNetV2	DenseNet 121	VGG16	**CRCCN-Net**
Acc (%)	95.28	94.46	96.44	97.64	99.21
Sen (%)	95.48	95.78	95.92	96.88	98.23
Pre (%)	95.23	92.52	97.24	96.16	99.18
Spe (%)	97.46	93.88	97.98	98.48	99.80
FPR (%)	5.48	7.62	2.24	2.02	1.84
FNR (%)	5.12	4.28	4.68	3.78	2.29
F-1 Score	0.9535	0.9412	0.9657	0.9651	0.9870
AUC	0.9604	0.9562	0.9748	0.9782	0.9890

Table 7
Training time of different models.

Model	Approx. training time (Minute)		
	Dataset_1	Dataset_2	DatasetL_3
Xception	78	1848	2265
Inception-ResNetV2	75	1810	2180
DenseNet121	67	1730	2015
VGG16	200	4520	5164
CRCCN-Net	**58**	**1622**	**1810**

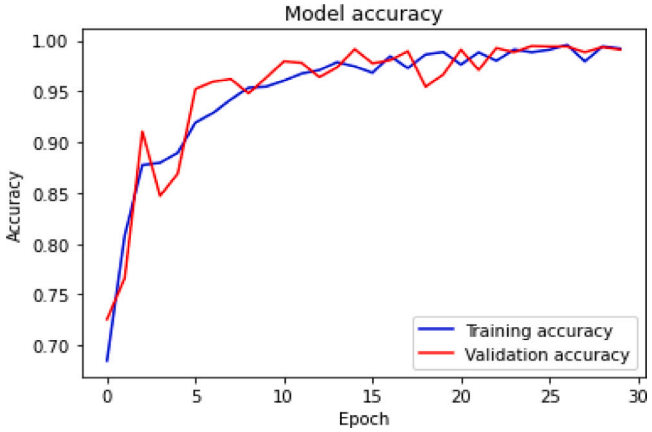

Fig. 13. CRCCN-Net training and validation accuracy on Dataset_3.

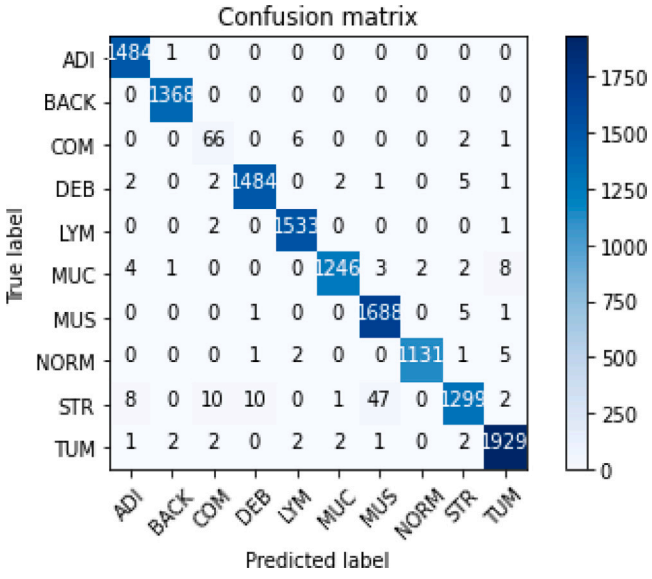

Fig. 14. Confusion matrices obtained from external test data using CRCCN-Net on Dataset_3.

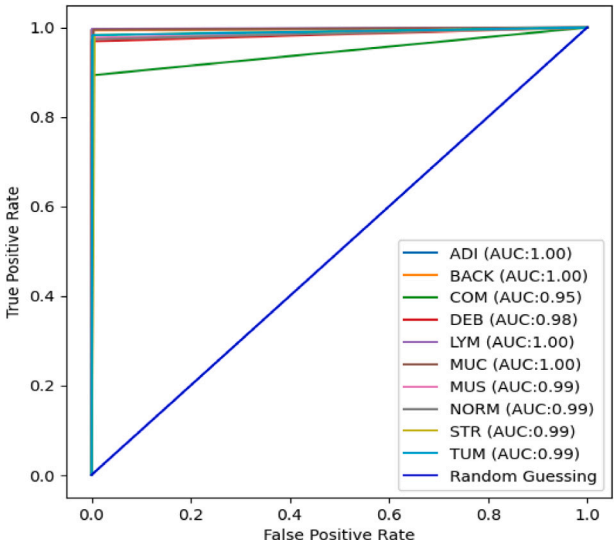

Fig. 15. Receiver operating characteristic of Dataset_3.

judgment and impart researchers to prospecting other hopes in the field of cancer research. The proposed model can be implemented on the hardware. The obtained results indicate that the developed CRCCN-Net performs better than other pre-trained models, with the minimum number of layers to classify colorectal tissue using HIs more accurately. The effectiveness of the proposed method with other state-of-the-art is demonstrated in Table 8.

Liang et al. [28] have developed MFF-CNN using shearlet transform for the identification of colon cancer. Adam optimizer had been utilized to minimize the loss. They used an initial learning rate of 0.001 and a batch size of 64. Their methods reduced false positive and false negative rates to 2.5%, and 5.5%, respectively. Their proposed MFF-CNN achieved Sen of 94.50%, Acc of 96%, Pre of 97.42%, F-1 score of 0.9554, Spe of 97.50%, and an AUC of 0.9600. They used only 8000 images (for training, testing, and validation) out of 100 K images while the proposed method used all images from the dataset and considered all classes of colorectal tissue.

Wang et al. [26] have proposed bilinear CNN to classify multi-class colorectal tissue. Bilinear CNN consists of two CNNs, whose CL outcomes are multiplied with an outer product at every spatial location [26]. The parameters used in their methods had been trained by

Table 8
Performance comparison of CRCCN-Net with the existing state of art on the same dataset for colorectal cancer classification.

Authors	Method	Acc (%)	Sen (%)	Pre (%)	Spe (%)	F-1 Score	AUC
Liang et al. [28]	MFF-CNN	96.00	94.05	97.42	97.50	0.9594	0.9600
Wang et al. [26]	Bilinear CNN	92.60	92.80	__	98.90	__	0.9850
Kather et al. [27]	TL+CNN	94.30	92.33	94.33	99.44	__	**0.9950**
Ghosh et al. [29] (Dataset_1)	EnsembleDNN	92.83	93.11	92.83	92.54	0.9283	0.9283
Ghosh et al. [29] (Dataset_2)	EnsembleDNN	96.16	96.15	96.17	96.17	0.9616	0.9616
Ghosh et al. [29] (Dataset_3)	EnsembleDNN	99.13	97.85	99.10	99.64	0.9847	0.9875
Proposed (Dataset_1)	**CRCCN-Net**	93.50	93.62	94.12	99.06	0.9386	0.9562
(Dataset_2)	**CRCCN-Net**	96.26	96.34	96.44	99.52	0.9638	0.9800
(Dataset_3)	**CRCCN-Net**	**99.21**	**98.23**	**99.18**	**99.80**	**0.9870**	0.9890

the back-propagation algorithm. Their method achieved a classification Acc of 92.60%, Sen of 92.80%, Spe of 98.90%, and AUC of 0.9850.

Kather et al. [27] have suggested five pre-trained models for the classification of multi-class colorectal tissue using HIs. Their method had performed on a single dataset. Out of five pre-trained models, VGG19 achieved Acc of 94.30%, Sen of 92.33%, Pre of 94.33%, Spe of 99.44%, and AUC of 0.9950 on the external test dataset for the classification of colorectal tissue. In [27], misclassifications between MUS, STR, LYM, and DEB classes, were the most common. The proposed technique, on the other hand, minimized the misclassification of these classes.

The method proposed by Ghosh et al. [29] used two different datasets, to classify multi-class colorectal tissue HIs. They compared their proposed ensemble DNN along with three pre-trained models in terms of various performance matrices. Adam optimizer was used to update the weights for all models. Ensemble DNN achieved Acc of 92.83%, Pre of 92.83%, Sen of 93.11%, Spe of 92.54%, and F-1 score of 0.9283, on Dataset_1. Their method achieved Acc of 96.16%, Sen of 96.15%, Pre of 96.17%, Spe of 96.17%, and F-1 score of 0.9610, on Dataset_2.

This study proposed the architecture of CRCCN-Net, to classify multi-class colorectal tissue from HIs more accurately. In this article, the performance of the proposed network is compared with Xception, InceptionResNetV2, DenseNet121, and VGG16, on two different and merged datasets. CRCCN-Net achieved the classification Acc of 93.50%, 96.26%, and 99.21% using Dataset_1, Dataset_2, and Dataset_3, respectively. Xception achieved the classification Acc of 88.20%, 94.18%, and 95.28% using Dataset_1, Dataset_2, and Dataset_3, respectively. InceptionResNetV2 achieved the classification Acc of 89.20% using Dataset_1, 91.26% using Dataset_2, and 94.46% using Dataset_3. DenseNet121 achieved the classification Acc of 87.20%, 92.34%, and 96.44% using Dataset_1, Dataset_2, and Dataset_3, respectively. VGG16 achieved the classification Acc of 90.40% using Dataset_1, 95.74% using Dataset_2, and 97.64% using Dataset_3.

From the above discussion, it is clear that the proposed network with HIs performs better than Xception, InceptionResNetV2, DenseNet121, and VGG16. CRCCN-Net on Dataset_1 achieved Sen, Pre, Spe, and F-1 score of 93.62%, 94.12%, 99.06%, and 0.9386, respectively. On Dataset_2, CRCCN-Net achieved Sen of 96.34%, Pre of 96.44%, Spe of 99.52%, and F-1 score of 0.9638. The proposed network achieved Sen, pre, Spe, and F-1 score of 98.23%, 99.18%, 99.80%, and 0.9870, respectively on Dataset_3. The results of Table 8 represent that, CRCCN-Net outperformed other existing methods on the same dataset for the classification of colorectal tissue. It can be noted from the findings that CRCCN-Net can extract more accurate and effective features from HIs on diverse datasets related to colorectal tissue. Also, the proposed method reduced computational time complexity as compared to other pre-trained models used in this work.

The advantages of CRCCN-Net are listed below:

- CRCCN-Net is computationally fast as compared to pre-trained models used in this work.
- CRCCN-Net tackles CRC diagnosis strategically as compared to existing methods.
- Simple and less complex as it uses a comparatively less number of learnable parameters than pre-trained networks.
- CRCCN-Net is robust as it performs better than other existing methods on diverse datasets.

The limitations of CRCCN-Net are listed below:

- Due to limitations of the dataset, it has not been tested on other HIs such as prostate, adrenal, and liver.
- Requires more epochs for the less number of training samples.

Furthermore, the proposed CRCCN-Net is trained from scratch and performs better than other existing DL-based models for the colorectal tissue HIs classification. This work used only the HIs dataset to validate the proposed model. The proposed network can also evaluate the performance of the model on different types of images, such as X-rays, computed tomography, ultrasound, magnetic resonance imaging, etc.

5.1. Additional experiment on lung cancer dataset

This dataset [48] consists 15,000 HIs of lung tissues. All images are the size of 768 × 768 pixels. The dataset comprises three classes each having 5,000 HIs. Three defined classes are lung benign tissue, lung adenocarcinoma, and lung squamous cell carcinoma. Before being given as an input to CRCCN-Net, all HIs are resized to 150 × 150. The patch for each class is shown in Fig. 16. The robustness of the developed CRCCN-Net has also been tested on the lung cancer dataset to classify lung tissues into multiple classes. Table 9 depicts the performance comparison of CRCCN-Net with the existing methodology for the classification of lung cancer using HIs.

Hatuwal et al. [49] have proposed a CNN for the detection and classification of lung tissue HIs. The paper did not provide clear information about the CNN architecture. Li et al. [50] have developed an ML-based approach to classify lung cancer using HIs. They extracted multidimensional features based on edges and textures. The extracted features had given to SVM classifier for the classification of lung tissues. CRCCN-Net achieved an Acc of 98.30%, Sen of 98.16%, Pre of 97.84%, F-1 score of 0.9799, and AUC of 0.9860 for the classification of lung tissues. The results of Table 9 represent that CRCCN-Net outperformed other existing methods to classify lung tissues using HIs. It can be noted from the findings that CRCCN-Net can extract more accurate and effective features from HIs on diverse datasets. The proposed CRCCN-Net may also be used to detect and classify different types of cancer tissues such as prostate, skin, breast, liver, and other health-related abnormalities.

6. Conclusion

CRC stands third among cancer types in terms of severity and fatality worldwide. The most critical stage across every malignancy is early

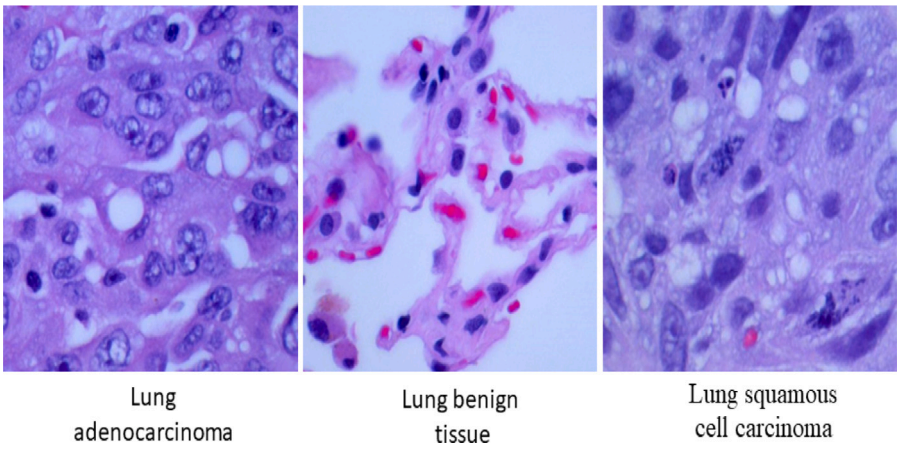

Fig. 16. Depiction of three class lung tissues.

Table 9
Performance comparison of CRCCN-Net with the existing state-of-the-art for lung cancer classification.

Authors	Method	Acc (%)	Sen (%)	Pre (%)	F-1 Score	AUC
Hatuwal et al. [53]	CNN	97.20	97.33	97.33	97.33	–
Li et al. [54]	ML	83.91	–	–	–	0.8250
Proposed	**CRCCN-Net**	**98.30**	**98.16**	**97.84**	**0.9799**	**0.9860**

and accurate diagnosis of CRC. In this study, CRCCN-Net is proposed for the automatic classification of colorectal tissue HIs. Four pre-trained models, namely, Xception, InceptionResNetV2, DenseNet121, VGG16, and proposed CRCCN-Net have been compared in terms of various performance metrics. Developed CRCCN-Net obtained the highest classification Acc of 99.21%, Sen of 98.23%, Pre of 99.18%, Spe of 99.80%, and F-1 score of 0.9870. The results indicate that the proposed CRCCN-Net is computationally fast and efficient than pre-trained models for the classification of colorectal tissue. The robustness of the proposed CRCCN-Net has also been tested on the lung cancer dataset to classify lung tissue into multiple classes. Developed CRCCN-Net is available for testing with other HIs datasets. In the future, the robustness of the proposed model will be validated on different types of images, such as X-rays, computed tomography, ultrasound, magnetic resonance imaging, etc. The proposed network can be extended to optimize the hyperparameters using a suitable optimization algorithm.

CRediT authorship contribution statement

Anurodh Kumar: Conception and design of study, Acquisition of data, Analysis and/or interpretation of data, Writing – original draft, Writing – review & editing. **Amit Vishwakarma:** Conception and design of study, Analysis and/or interpretation of data, Writing – original draft, Writing – review & editing. **Varun Bajaj:** Analysis and/or interpretation of data, Writing – original draft, Writing – review & editing.

Declaration of competing interest

The authors declare that they have no known competing financial interests or personal relationships that could have appeared to influence the work reported in this paper.

Data availability

Data will be made available on request.

Acknowledgment

All authors approved version of the manuscript to be published.

References

[1] H. Sung, J. Ferlay, R.L. Siegel, M. Laversanne, I. Soerjomataram, A. Jemal, F. Bray, Global cancer statistics 2020: GLOBOCAN estimates of incidence and mortality worldwide for 36 cancers in 185 countries, CA: Cancer J. Clin. 71 (3) (2021) 209–249.

[2] R.L. Siegel, K.D. Miller, H.E. Fuchs, A. Jemal, Cancer statistics, 2022, CA: Cancer J. Clin. (2022).

[3] J.G. Elmore, G.M. Longton, P.A. Carney, B.M. Geller, T. Onega, A.N. Tosteson, H.D. Nelson, M.S. Pepe, K.H. Allison, S.J. Schnitt, et al., Diagnostic concordance among pathologists interpreting breast biopsy specimens, JAMA 313 (11) (2015) 1122–1132.

[4] G. Litjens, T. Kooi, B.E. Bejnordi, A.A.A. Setio, F. Ciompi, M. Ghafoorian, J.A. Van Der Laak, B. Van Ginneken, C.I. Sánchez, A survey on deep learning in medical image analysis, Med. Image Anal. 42 (2017) 60–88.

[5] S. Waite, J.M. Scott, A. Legasto, S. Kolla, B. Gale, E.A. Krupinski, Systemic error in radiology, Am. J. Roentgenol. 209 (3) (2017) 629–639.

[6] S. Aydın, Ç. Güdücü, F. Kutluk, A. Öniz, M. Özgören, The impact of musical experience on neural sound encoding performance, Neurosci. Lett. 694 (2019) 124–128.

[7] V. Bajaj, M. Pawar, V.K. Meena, M. Kumar, A. Sengur, Y. Guo, Computer-aided diagnosis of breast cancer using bi-dimensional empirical mode decomposition, Neural Comput. Appl. 31 (8) (2019) 3307–3315.

[8] S. Aydın, Cross-validated adaboost classification of emotion regulation strategies identified by spectral coherence in resting-state, Neuroinformatics (2021) 1–13.

[9] J. Amin, M. Sharif, M. Raza, T. Saba, M.A. Anjum, Brain tumor detection using statistical and machine learning method, Comput. Methods Programs Biomed. 177 (2019) 69–79.

[10] A. Tabesh, M. Teverovskiy, H.-Y. Pang, V.P. Kumar, D. Verbel, A. Kotsianti, O. Saidi, Multifeature prostate cancer diagnosis and Gleason grading of histological images, IEEE Trans. Med. Imaging 26 (10) (2007) 1366–1378.

[11] L. Alzubaidi, J. Zhang, A.J. Humaidi, A. Al-Dujaili, Y. Duan, O. Al-Shamma, J. Santamaría, M.A. Fadhel, M. Al-Amidie, L. Farhan, Review of deep learning: Concepts, CNN architectures, challenges, applications, future directions, J. Big Data 8 (1) (2021) 1–74.

[12] S. Aydın, Deep learning classification of neuro-emotional phase domain complexity levels induced by affective video film clips, IEEE J. Biomed. Health Inf. 24 (6) (2019) 1695–1702.

[13] S.R. Nayak, D.R. Nayak, U. Sinha, V. Arora, R.B. Pachori, Application of deep learning techniques for detection of COVID-19 cases using chest X-ray images: A comprehensive study, Biomed. Signal Process. Control 64 (2021) 102365.

[14] J.S. Khan, M. Kaushik, A. Chaurasia, M.K. Dutta, R. Burget, Cardi-net: A deep neural network for classification of cardiac disease using phonocardiogram signal, Comput. Methods Programs Biomed. 219 (2022) 106727.

[15] K. Gupta, V. Bajaj, I.A. Ansari, An improved deep learning model for automated detection of BBB using ST spectrograms of smoothed VCG signal, IEEE Sens. J. (2022).

[16] P. Dhar, S. Dutta, V. Mukherjee, Cross-wavelet assisted convolution neural network (AlexNet) approach for phonocardiogram signals classification, Biomed. Signal Process. Control 63 (2021) 102142.
[17] N. Cinar, A. Ozcan, M. Kaya, A hybrid DenseNet121-unet model for brain tumor segmentation from MR images, Biomed. Signal Process. Control 76 (2022) 103647.
[18] I.A. Bratchenko, L.A. Bratchenko, Y.A. Khristoforova, A.A. Moryatov, S.V. Kozlov, V.P. Zakharov, Classification of skin cancer using convolutional neural networks analysis of Raman spectra, Comput. Methods Programs Biomed. (2022) 106755.
[19] T.-L. Nguyen, S. Kavuri, S.-Y. Park, M. Lee, Attentive hierarchical ANFIS with interpretability for cancer diagnostic, Expert Syst. Appl. (2022) 117099.
[20] S. Rathore, M. Hussain, A. Khan, Automated colon cancer detection using hybrid of novel geometric features and some traditional features, Comput. Biol. Med. 65 (2015) 279–296.
[21] G. Olgun, C. Sokmensuer, C. Gunduz-Demir, Local object patterns for the representation and classification of colon tissue images, IEEE J. Biomed. Health Inf. 18 (4) (2013) 1390–1396.
[22] D. Altunbay, C. Cigir, C. Sokmensuer, C. Gunduz-Demir, Color graphs for automated cancer diagnosis and grading, IEEE Trans. Biomed. Eng. 57 (3) (2009) 665–674.
[23] C.-A. Weis, J.N. Kather, S. Melchers, H. Al-Ahmdi, M.J. Pollheimer, C. Langner, T. Gaiser, Automatic evaluation of tumor budding in immunohistochemically stained colorectal carcinomas and correlation to clinical outcome, Diagnostic Pathol. 13 (1) (2018) 1–12.
[24] K. Sirinukunwattana, S.E.A. Raza, Y.-W. Tsang, D.R. Snead, I.A. Cree, N.M. Rajpoot, Locality sensitive deep learning for detection and classification of nuclei in routine colon cancer histology images, IEEE Trans. Med. Imaging 35 (5) (2016) 1196–1206.
[25] C.T. Sari, C. Gunduz-Demir, Unsupervised feature extraction via deep learning for histopathological classification of colon tissue images, IEEE Trans. Med. Imaging 38 (5) (2018) 1139–1149.
[26] C. Wang, J. Shi, Q. Zhang, S. Ying, Histopathological image classification with bilinear convolutional neural networks, in: 2017 39th Annual International Conference of the IEEE Engineering in Medicine and Biology Society, EMBC, IEEE, 2017, pp. 4050–4053.
[27] J.N. Kather, J. Krisam, P. Charoentong, T. Luedde, E. Herpel, C.-A. Weis, T. Gaiser, A. Marx, N.A. Valous, D. Ferber, et al., Predicting survival from colorectal cancer histology slides using deep learning: A retrospective multicenter study, PLoS Med. 16 (1) (2019) e1002730.
[28] M. Liang, Z. Ren, J. Yang, W. Feng, B. Li, Identification of colon cancer using multi-scale feature fusion convolutional neural network based on shearlet transform, IEEE Access 8 (2020) 208969–208977.
[29] S. Ghosh, A. Bandyopadhyay, S. Sahay, R. Ghosh, I. Kundu, K. Santosh, Colorectal histology tumor detection using ensemble deep neural network, Eng. Appl. Artif. Intell. 100 (2021) 104202.
[30] A.B. Hamida, M. Devanne, J. Weber, C. Truntzer, V. Derangère, F. Ghiringhelli, G. Forestier, C. Wemmert, Deep learning for colon cancer histopathological images analysis, Comput. Biol. Med. 136 (2021) 104730.
[31] H. Chen, C. Li, X. Li, M.M. Rahaman, W. Hu, Y. Li, W. Liu, C. Sun, H. Sun, X. Huang, et al., IL-MCAM: An interactive learning and multi-channel attention mechanism-based weakly supervised colorectal histopathology image classification approach, Comput. Biol. Med. 143 (2022) 105265.
[32] P. Sabol, P. Sinčák, P. Hartono, P. Kočan, Z. Benetinová, A. Blichárová, L. Verbóová, E. Štammová, A. Sabolová-Fabianová, A. Jašková, Explainable classifier for improving the accountability in decision-making for colorectal cancer diagnosis from histopathological images, J. Biomed. Inform. 109 (2020) 103523.
[33] M.S. Kwak, H.H. Lee, J.M. Yang, J.M. Cha, J.W. Jeon, J.Y. Yoon, H.I. Kim, Deep convolutional neural network-based lymph node metastasis prediction for colon cancer using histopathological images, Front. Oncol. 10 (2021) 3053.
[34] E.F. Ohata, J.V.S.d. Chagas, G.M. Bezerra, M.M. Hassan, V.H.C. de Albuquerque, et al., A novel transfer learning approach for the classification of histological images of colorectal cancer, J. Supercomput. 77 (9) (2021) 9494–9519.
[35] K.-S. Wang, G. Yu, C. Xu, X.-H. Meng, J. Zhou, C. Zheng, Z. Deng, L. Shang, R. Liu, S. Su, et al., Accurate diagnosis of colorectal cancer based on histopathology images using artificial intelligence, BMC Med. 19 (1) (2021) 1–12.
[36] A. Davri, E. Birbas, T. Kanavos, G. Ntritsos, N. Giannakeas, A.T. Tzallas, A. Batistatou, Deep learning on histopathological images for colorectal cancer diagnosis: A systematic review, Diagnostics 12 (4) (2022) 837.
[37] J.N. Kather, C.-A. Weis, F. Bianconi, S.M. Melchers, L.R. Schad, T. Gaiser, A. Marx, F.G. Zöllner, Multi-class texture analysis in colorectal cancer histology, Sci. Rep. 6 (1) (2016) 1–11.
[38] J.N. Kather, N. Halama, A. Marx, 100,000 Histological images of human colorectal cancer and healthy tissue, vol. 1214456, 2018, http://dx.doi.org/10.5281/Zenodo.
[39] F. Chollet, Xception: Deep learning with depthwise separable convolutions, in: Proceedings of the IEEE Conference on Computer Vision and Pattern Recognition, 2017, pp. 1251–1258.
[40] C. Szegedy, S. Ioffe, V. Vanhoucke, A.A. Alemi, Inception-v4, inception-resnet and the impact of residual connections on learning, in: Thirty-First AAAI Conference on Artificial Intelligence, 2017.
[41] G. Huang, Z. Liu, L. Van Der Maaten, K.Q. Weinberger, Densely connected convolutional networks, in: Proceedings of the IEEE Conference on Computer Vision and Pattern Recognition, 2017, pp. 4700–4708.
[42] M.Z. Alom, T.M. Taha, C. Yakopcic, S. Westberg, P. Sidike, M.S. Nasrin, B.C. Van Esesn, A.A.S. Awwal, V.K. Asari, The history began from alexnet: A comprehensive survey on deep learning approaches, 2018, arXiv preprint arXiv:1803.01164.
[43] F.N. Iandola, S. Han, M.W. Moskewicz, K. Ashraf, W.J. Dally, K. Keutzer, SqueezeNet: AlexNet-level accuracy with 50x fewer parameters and< 0.5 MB model size, 2016, arXiv preprint arXiv:1602.07360.
[44] S.K. Khare, V. Bajaj, Time-frequency representation and convolutional neural network-based emotion recognition, IEEE Trans. Neural Netw. Learn. Syst. (2020).
[45] S. Bhalerao, I.A. Ansari, A. Kumar, D.K. Jain, A reversible and multipurpose ECG data hiding technique for telemedicine applications, Pattern Recognit. Lett. 125 (2019) 463–473.
[46] D. Soydaner, A comparison of optimization algorithms for deep learning, Int. J. Pattern Recognit. Artif. Intell. 34 (13) (2020) 2052013.
[47] N. Srivastava, G. Hinton, A. Krizhevsky, I. Sutskever, R. Salakhutdinov, Dropout: a simple way to prevent neural networks from overfitting, J. Mach. Learn. Res. 15 (1) (2014) 1929–1958.
[48] A.A. Borkowski, M.M. Bui, L.B. Thomas, C.P. Wilson, L.A. DeLand, S.M. Mastorides, Lung and colon cancer histopathological image dataset (lc25000), 2019, arXiv preprint arXiv:1912.12142.
[49] B.K. Hatuwal, H.C. Thapa, Lung cancer detection using convolutional neural network on histopathological images, Int. J. Comput. Trends Technol. 68 (2020) 21–24.
[50] M. Li, X. Ma, C. Chen, Y. Yuan, S. Zhang, Z. Yan, C. Chen, F. Chen, Y. Bai, P. Zhou, et al., Research on the auxiliary classification and diagnosis of lung cancer subtypes based on histopathological images, IEEE Access 9 (2021) 53687–53707.